Submitted Manuscript: Confidential

Ideal Weyl points and helicoid surface states in artificial photonic crystal structures

Authors: Biao Yang[1†], Qinghua Guo[1, 4†], Ben Tremain[2†], Rongjuan Liu[3†], Lauren E. Barr[2],

Qinghui Yan[3], Wenlong Gao[1], Hongchao Liu[1], Yuanjiang Xiang[4], Jing Chen[5], Chen Fang[3],

Alastair Hibbins[2]*, Ling Lu[3]*, Shuang Zhang[1]*

Affiliations:

[1] School of Physics and Astronomy, University of Birmingham, Birmingham B15 2TT, United

Kingdom.

[2] Electromagnetic and Acoustic Materials Group, Department of Physics and Astronomy,

University of Exeter, Stocker Road, Exeter EX4 4QL, United Kingdom.

[3] Institute of Physics, Chinese Academy of Sciences/Beijing National Laboratory for Condensed

Matter Physics, Beijing 100190, China

[4] Key Laboratory of Optoelectronic Devices and Systems of Ministry of Education and

Guangdong Province, College of Optoelectronic Engineering, Shenzhen University, Shenzhen

518060, China.

[5] School of Physics, Nankai University, Tianjin 300071, China

*Correspondence to: A.P.Hibbins@exeter.ac.uk; linglu@iphy.ac.cn; s.zhang@bham.ac.uk

†These authors contributed equally to this work.

Abstract: Weyl points are the crossings of linearly dispersing energy bands of three-dimensional crystals, providing the opportunity to explore a variety of intriguing phenomena such as topologically protected surface states and chiral anomalies. However, the lack of an ideal Weyl system in which the Weyl points all exist at the same energy and are separated from any other bands, poses a serious limitation to the further development of Weyl physics and potential applications. By experimentally characterizing a microwave photonic crystal of saddle-shaped metallic coils, we observe ideal Weyl points that are related to each other through symmetry operations. Topological surface states exhibiting helicoidal structure have also been demonstrated. Our system provides a photonic platform for exploring ideal Weyl systems and developing possible topological devices.

One Sentence Summary: An ideal Weyl system and helicoid surface states are observed in a designed microwave photonic crystal structure.

Main Text: Topology is the mathematics of conserved properties under continuous deformations, and the recent study of band topologies is yielding a suite of fascinating interface transport phenomena that include one-way propagation of energy and novel relativistic behavior. The two-dimensional honeycomb lattice is the most studied in the exploration of topological phenomena. Made famous by graphene (*1*), the energy-momentum dispersion in a honeycomb system is linear, and the crossings of bands in energy-momentum space are known as Dirac points. The transport of the quasi-particles around these points is massless, and this remarkable transport behavior is associated with the 'hidden' symmetry associated with its two identical sub-lattices. Weyl points are the characteristic of an analogous phenomenon when the lattice is extended to three dimensions (*2-5*). In electronic systems, materials exhibiting Weyl points are known as Weyl semimetals, and Weyl fermion is the solution to the massless Dirac equation. Each Weyl point can be assigned an integer 'charge' based of its chirality, known as the Chern number, and much like magnetic monopoles, Weyl points are only ever found in pairs of opposite charge. Just like Dirac points these Weyl points also exist in photonic systems, but unlike Dirac points, they can only exist once either (or both) time-reversal or space-inversion symmetry of the crystal is broken. To date, Weyl points of various forms have been proposed and realized in several boson or fermion systems (*2-4, 6-13*). Among them, the presence of surface state arcs as one of the fingerprints of Weyl systems has been observed.

However, demonstration of more fundamental topological features of Weyl points, such as the helicoidal dispersion, which yield the open Fermi arcs of topological surface states (*14*), have been hindered by the complicated configuration of energy bands at the Weyl energy. Moreover, some realistic and innovative device applications critically depend on a simple embodiment of

Weyl systems (*5*). Thus, an ideal Weyl system (*15-17*), has attracted much attention, because in such system all Weyl nodes are symmetry-related, residing at the same energy with a large momentum separation, and devoid of non-topological bands in a sufficiently large energy interval.

While Weyl degeneracies can be readily found by breaking either time-reversal or inversion symmetry (*5*) (or both), the experimental realization of a truly ideal Weyl system has not yet been reported. Here, we explore the microwave response of a three-dimensional photonic crystal comprised of metallic inclusions (termed a 'meta-crystal') in order to realize ideal Weyl system protected by D_{2d} point symmetry. Our meta-crystal exhibits four Weyl points at the same energy, the minimum number allowed in the presence of time-reversal symmetry. By placing an excitation point-source on one surface of the crystal, and scanning the near-fields on the opposite surface, we observe the intriguing helicoidal structure of topological surface states: a physical representation of Riemann surface generated by a multi-valued function (*14*).

Our meta-crystal design offers an ideal platform for investigating various unconventional physics in Weyl systems. The symmetry of the studied meta-crystal belongs to the simple tetragonal lattice with symmorphic space group $P\bar{4}m2$ (No. 115). The basis comprises of a saddle-shaped connective metallic coil (Fig. 1A and B) that possesses D_{2d} ($\bar{4}2m$ in Hermann-Mauguin notation) point group symmetry. The system has no spatial inversion. These metallic elements support localized electromagnetic resonances with current distributions that can be expanded into multipolar modes (*18*). In an effective medium model [Sec. 4, Fig. S1, (*19*)], these resonances collectively exhibit bi-anisotropic effect, leading to a directionally dependent chirality response (*20*). Here, the unavoidable crossings between the longitudinal mode (LM) with negative dispersion and the transverse electric modes (TM) with positive dispersion along

Γ–M result in the formation of a type-I Weyl point as shown in Fig. 1C [Fig. S2, (*19*)] (*21*). Analysis via the irreducible representation of the point group shows that these two modes belong to two different classes, with eigenvalues ±1 of C_2 rotation along Γ-M (Fig. 1D), where level repulsion is forbidden [Sec. 5, Fig. S3, (*19*)]. The other three Weyl points are obtained after application of the D_{2d} symmetry operation. For instance, three two-fold rotation symmetries (C_2 and $2C_2$') combined with time-reversal symmetry guarantee that these four Weyl nodes are located on the Γ–M at the same frequency, where application of two mirror symmetries (σ_x and σ_y) reverse the corresponding topological charges. Figure 1E shows the simulated band structure along high symmetry lines (as defined in Fig. 1D) in the Brillouin zone (BZ), where a pair of Weyl points reside at the same frequency. As such, these Weyl degeneracies appear in a relatively large energy window (~2.1 GHz around frequency of the Weyl point, cyan shadow region) that is also devoid of other bulk bands, and hence unequivocally facilitates their experimental identification.

The linear band crossings of the surface states around the Weyl point are confirmed by angle resolved transmission measurements (*9*). In order to couple energy across the meta-crystal, the momentum of the surface states must be matched to the smaller in-plane momentum of an incident wave, a sample with special crystal-cutting is fabricated (Fig. 2A), where the crystal orientation forms an angle of 26.57° with one of the cutting boundaries. Compared with the global axis, xyz, a local coordinate, uvw, is defined. The length (along u), width (along v) and height (along w) of the sample are 300 mm, 100 mm and 300 mm, respectively. Two angles, θ and ϕ (Fig. 2A and B), are scanned to obtain the angle-resolved transmission spectrum. With this specific crystal cutting, when $\phi = 0°$ Weyl points in BZ are projected along the scan wavevector k_p, which is related to θ as indicated in Fig. 2C. Obviously, two of the projected Weyl points are

located within the light circle (magenta circle) at the Weyl frequency (13.5 GHz). Thus, even a plane wave illuminated directly from air onto the sample can address these two Weyl points. Comparisons between the simulation and experiment results are shown in Fig. 2D, E and F. In Fig. 2D, with $\phi = 0°$, a linear gapless energy dispersion is obtained and the density of states vanishes at the Weyl frequency due to the absence of other bulk states at the same frequency in an ideal Weyl system. After rotating the sample to $\phi = 30°$ and $60°$ around the v-axis, a complete gap is observed as expected.

Another direct manifestation of the topological aspects of Weyl system is the exotic topological surface states taking the form of arcs connecting the topologically distinct bulk states. Following a closed contour around an end of the arcs, one moves between the lower ('valence') and upper ('conduction') bands (14), which is a direct consequence of the chiral characteristic of Weyl nodes, as schematically shown in Fig. 3A. It is well known that the gapless surface states of Weyl crystals take the form of helicoid Riemann surfaces (14), where the bulk Weyl points correspond to the poles and zeros adopting the sign of their respective Chern numbers. Recently, it was shown that topological surface states of double Weyl systems can be analytically expressed, across the entire Brillouin zone, as the double-periodic Weierstrass elliptic function (22). Since the Weierstrass elliptic function has one second-order pole and one second-order zero, it is not the most fundamental expression of the Weyl surfaces states. Here, we show that our ideal-Weyl meta-crystal of four Weyl points has surface states whose dispersion is topologically equivalent to the imaginary part of Jacobi elliptic function cn(z,m) of two poles and two zeros on the complex plane. cn(z,m) is a meromorphic function with periods $4K(m)$ and $4K(1-m)$, where K is the complete elliptic integrals of the first kind. For our system, the mapping is given by $\omega(k_x,k_y) \sim$ cn$((k_x-k_y)/2+(k_x+k_y)i/2,1/2)$, as plotted in Fig. 3A.

The helicoidal structure of the surface arcs were probed using the transmitted near-field scanning configuration with the excitation source located at the center of the bottom layer of the meta-crystal stack (Fig. 3B, setup 'a'), where the detecting probe can raster-scan the top surface to map out both the bulk and surface modes. Another configuration (setup 'b' as shown in Fig. S4B), in which the excitation source is positioned at the edge or corner of the top surface, is also used to identify the surface states. These two setups provide complementary information for the observation of helicoid surface states. In all near field measurements, we set the scanning step as 1 mm (a /3), providing a large surface momentum space in the range of $[-3\pi/a, 3\pi/a]^2$ after the Fourier transformation. The helicoid structure of surface arc is experimentally measured and numerically simulated, and is presented as a series of equi-frequency contours between 12.6 GHz and 14.0 GHz (Fig. 3C and 3E in experiment, and Fig. 3D and 3F in simulation).

As shown in Fig. 3C and D, at 13.1 GHz, which is below the Weyl frequency, the Fourier transformation of the experimentally measured field distribution shows the presence of four symmetrically displaced elliptical bulk states with the same size located along the diagonal directions. We clearly observe two surface arcs running across the Brillouin zone boundaries and connecting the neighboring bulk states with opposite topological charges. In the vicinity of the air equi-frequency contour (circle), there exists a surface ellipse. The surface ellipse joins and reroutes the surface arc at higher frequencies (Fig. 3E and F). Indeed, the surface ellipse and surface arcs together form the same unified helicoid surface in the dispersion of the surface states.

With increasing frequency, the top surface arc emerged from the Weyl node with positive / negative topological charge rotates anti-clockwise / clockwise. The observed rotation of the helicoid surface state around a Weyl node can therefore be used to detect the chirality of the Weyl node (23). At lower frequencies, as mentioned above each surface arc connect between the

bulk states through the Brillouin zone boundary, while the surface ellipse expands gradually with increasing frequency. Between 13.5 and 13.6 GHz, the surface arc and surface ellipse connect with each other, and then transition into a new configuration: a direct surface arc connecting between the bulk states within the Brillouin zone, and a surface ellipse centered at its edge. The evolution of the surface arc configuration across the measured frequency range matches topologically with that described by the Jacobi elliptic function shown in Fig. 3A. At the frequency of 14.3 GHz, the surface arcs appear to be linear [Fig. S4F, (*19*)], leading to nearly diffraction-less propagation of the surface wave in the real space [Fig. S4C, (*19*)]. Slightly away from the Weyl frequency, the equi-energy contour of the bulk state consists of four very small spheres enclosing the Weyl points. It is expected that the interference between them result in a chessboard like interference pattern in real space, which is experimentally confirmed as a spatial frequency filter (*17*) [Fig. S5, (*19*)]. In addition, the dimensional reduction from ideal Weyl points to graphene-like dispersion is shown in Fig. S6 [Sec. 8, (*19*)]. We also analyzed that the presence of dielectric loss of our system does not affect the existence of the Weyl points [Sec. 9, (*19*)].

The designed ideal Weyl system presented here opens up opportunities for studying intriguing physics and offers a prototype platform for realistic device applications. In photonics, besides the topologically nontrivial surface states supported by Weyl materials, the diverging Berry curvature (*5*) close to Weyl points provide a new degree of freedom in controlling the transport of optical wave packets, and may lead to the observation of a gigantic Hall effect for light (*24*). Furthermore, any phenomena related to the conical dispersion of the light cone may be observed around Weyl points, such as diverging and diminishing scattering cross sections (*25*).

The vanishing density of states at Weyl frequencies also provides a robust platform for controlling light matter interaction when emitters are embedded inside photonic Weyl materials.

References and Notes

1.   A. H. Castro Neto, F. Guinea, N. M. R. Peres, K. S. Novoselov, A. K. Geim, The electronic properties of graphene. Reviews of Modern Physics 81, 109-162 (2009). https://doi.org/10.1103/RevModPhys.81.109

2.   X. Wan, A. M. Turner, A. Vishwanath, S. Y. Savrasov, Topological semimetal and Fermi-arc surface states in the electronic structure of pyrochlore iridates. Physical Review B 83, 205101 (2011). https://doi.org/10.1103/PhysRevB.83.205101

3.   A. A. Burkov, L. Balents, Weyl Semimetal in a Topological Insulator Multilayer. Phys. Rev. Lett. 107, 127205 (2011). https://doi.org/10.1103/PhysRevLett.107.127205

4.   G. Xu, H. Weng, Z. Wang, X. Dai, Z. Fang, Chern Semimetal and the Quantized Anomalous Hall Effect in HgCr2Se4. Phys. Rev. Lett. 107, 186806 (2011). https://doi.org/10.1103/PhysRevLett.107.186806

5.   N. P. Armitage, E. J. Mele, A. Vishwanath, Weyl and Dirac Semimetals in Three Dimensional Solids. arXiv:1705.01111 [cond-mat.str-el], (2017). https://arxiv.org/abs/1705.01111

6.   S.-Y. Xu et al., Discovery of a Weyl fermion semimetal and topological Fermi arcs. Science 349, 613 (2015). DOI: 10.1126/science.aaa9297

7.   H. Weng, C. Fang, Z. Fang, B. A. Bernevig, X. Dai, Weyl Semimetal Phase in Noncentrosymmetric Transition-Metal Monophosphides. Phys. Rev. X 5, 011029 (2015). https://doi.org/10.1103/PhysRevX.5.011029

8.   A. A. Soluyanov et al., Type-II Weyl semimetals. Nature 527, 495-498 (2015). doi:10.1038/nature15768

9.   L. Lu et al., Experimental observation of Weyl points. Science 349, 622-624 (2015). DOI: 10.1126/science.aaa9273

10.   L. Huang et al., Spectroscopic evidence for a type II Weyl semimetallic state in MoTe2. Nat. Mater. 15, 1155-1160 (2016). doi:10.1038/nmat4685

11.   W.-J. Chen, M. Xiao, C. T. Chan, Photonic crystals possessing multiple Weyl points and the experimental observation of robust surface states. Nat. Commun. 7, 13038 (2016). doi:10.1038/ncomms13038

12.   J. Noh et al., Experimental observation of optical Weyl points and Fermi arc-like surface states. Nat Phys 13, 611-617 (2017). doi:10.1038/nphys4072

13.   B. Yang et al., Direct observation of topological surface-state arcs in photonic metamaterials. Nature Communications 8, 97 (2017). doi:10.1038/s41467-017-00134-1

14.   C. Fang, L. Lu, J. Liu, L. Fu, Topological semimetals with helicoid surface states. Nat Phys 12, 936-941 (2016). doi:10.1038/nphys3782

15.   J. Ruan et al., Symmetry-protected ideal Weyl semimetal in HgTe-class materials. Nat Commun 7, 11136 (2016). doi:10.1038/ncomms11136

16.   J. Ruan et al., Ideal Weyl Semimetals in the Chalcopyrites CuTlSe2, AgTlTe2, AuTlTe2, and ZnPbAs2. Physical Review Letters 116, 226801 (2016). https://doi.org/10.1103/PhysRevLett.116.226801

17.   L. Wang, S.-K. Jian, H. Yao, Topological photonic crystal with equifrequency Weyl points. Physical Review A 93, 061801 (2016). https://doi.org/10.1103/PhysRevA.93.061801

18.   T. Kaelberer, V. A. Fedotov, N. Papasimakis, D. P. Tsai, N. I. Zheludev, Toroidal Dipolar Response in a Metamaterial. Science 330, 1510-1512 (2010). DOI: 10.1126/science.1197172

19.   Materials and methods are available as supplementary materials.

20.   Q. Guo, W. Gao, J. Chen, Y. Liu, S. Zhang, Line Degeneracy and Strong Spin-Orbit Coupling of Light with Bulk Bianisotropic Metamaterials. Physical Review Letters 115, 067402 (2015). https://doi.org/10.1103/PhysRevLett.115.067402

21.   M. Xiao, Q. Lin, S. Fan, Hyperbolic Weyl Point in Reciprocal Chiral Metamaterials. Phys. Rev. Lett. 117, 057401 (2016). https://doi.org/10.1103/PhysRevLett.117.057401

22.   T. Zhang et al., Double-Weyl phonons in transition-metal monosilicides. arXiv:1705.07244 [cond-mat.mtrl-sci], (2017). https://arxiv.org/abs/1705.07244

23.   Q. Ma et al., Direct optical detection of Weyl fermion chirality in a topological semimetal. Nature Physics 13, 842 (2017). doi:10.1038/nphys4146

24.   M. Onoda, S. Murakami, N. Nagaosa, Hall Effect of Light. Phys. Rev. Lett. 93, 083901 (2004). https://doi.org/10.1103/PhysRevLett.93.083901

25.   M. Zhou et al., Electromagnetic scattering laws in Weyl systems. Nature Communications 8, 1388 (2017). doi:10.1038/s41467-017-01533-0

26.   R. Zhao, T. Koschny, C. M. Soukoulis, Chiral metamaterials: retrieval of the effective parameters with and without substrate. Optics Express 18, 14553-14567 (2010). https://doi.org/10.1364/OE.18.014553

27.   A. Raman, S. Fan, Photonic Band Structure of Dispersive Metamaterials Formulated as a Hermitian Eigenvalue Problem. Physical Review Letters 104, 087401 (2010). https://doi.org/10.1103/PhysRevLett.104.087401
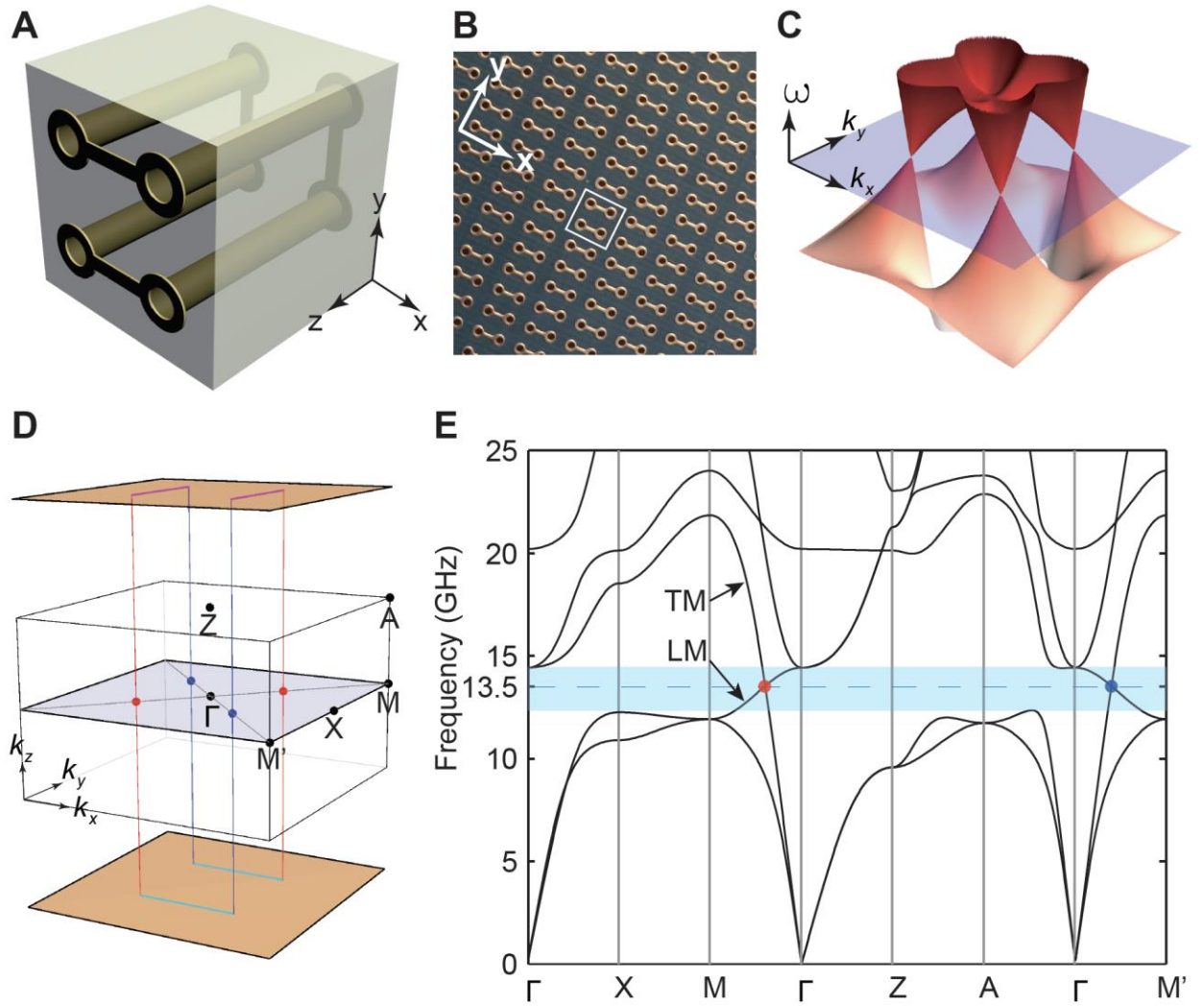
Fig. 1. Structure and band topology of the ideal photonic Weyl meta-crystal. (**A**) Schematic

of a saddle shaped metallic inclusion, which has non-centrosymmetric D$_{2d}$ point group

symmetry, embedded in a dielectric (dielectric constant of 2.2 ± 2% at 10 GHz). Here $a_x = a_y = a$

= 3 mm and a_z = 4.5 mm. (**B**) Photograph of the top surface of the sample, fabricated with

printed circuit board technology by etching 3 mm-thick double-sided, copper-clad (0.035 mm-thick) dielectric laminates. A 1.5 mm-thick 'blank' layer spaces each pair of printed layers to prevent electrical connection between the metallic coils. The bulk sample is assembled by stacking (1.5 + 3) mm bilayers in the z-direction. The unit cell is indicated by the white square. (**C**) Four type-I Weyl points reside on the same energy as indicated by the blue plane with respect of $k_z = 0$. (**D**) Bulk and surface Brillouin zone with four Weyl points located along the Γ–M directions. Top (magenta) and bottom (cyan) topological surface-state arcs are shown schematically. (**E**) CST Microwave Studio (CST) simulated band structure along high-symmetry lines. The cyan shaded area highlights the energy window where the ideal Weyl points (red / blue point) reside. Longitudinal (LM) and transverse modes (TM) are labelled.
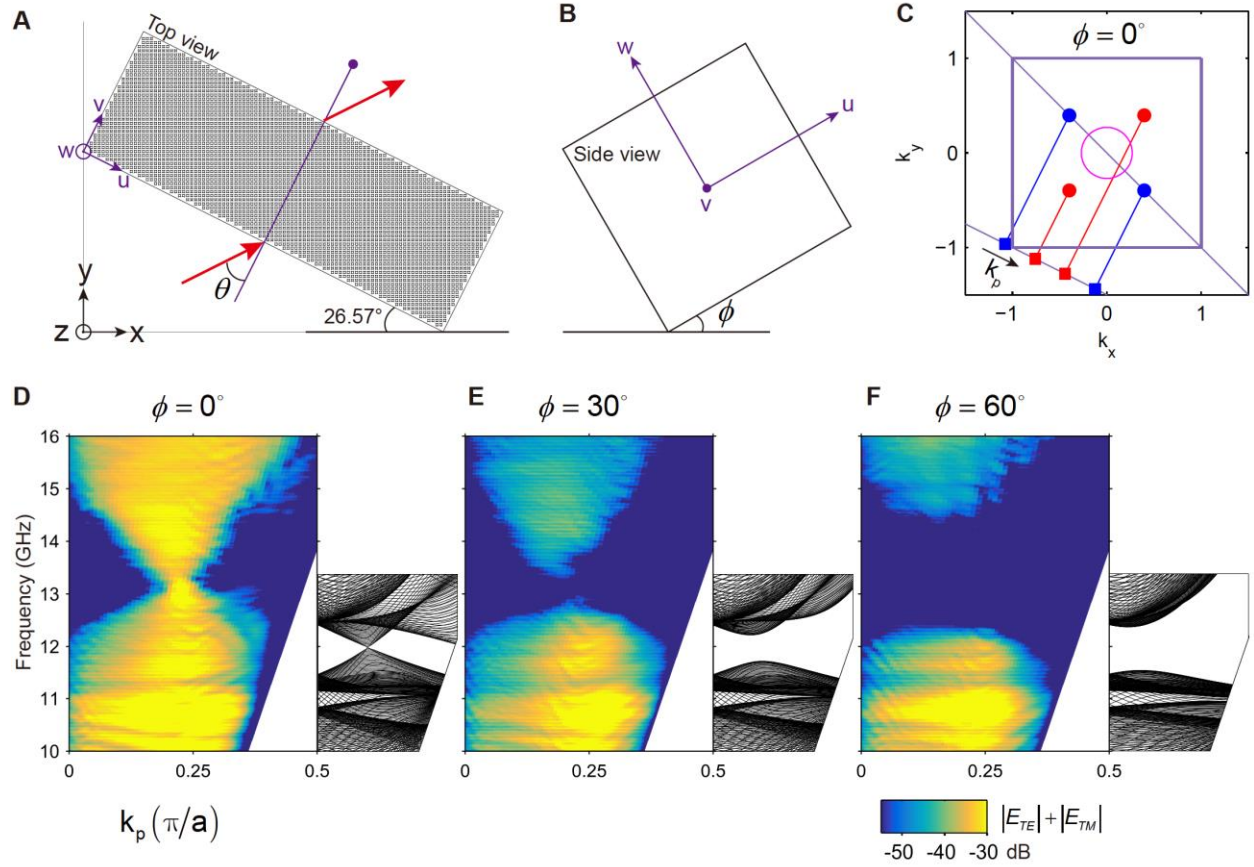
Fig. 2. Angle resolved transmission measurement of the ideal Weyl system. (A, B) Schematic view of the sample fabricated with crystal cutting angle of 26.57º; top and side views are illustrated. θ and ϕ are the scan and rotation angles defined along the local coordinates v and w, respectively. **(C)** Projection of Weyl points in momentum space with respect to the global coordinates (x, y, z) when $\phi = 0°$. First Brillouin zone is indicated by the purple square. Magenta circle indicates the equi-frequency contour of vacuum at 13.5 GHz. Under a fixed ϕ, k_p is the momentum associated with the scan angle θ (9). **(D)**, **(E)** and **(F)** are the band projections with ϕ = 0˚, 30˚ and 60˚, respectively. The experimental and simulated results are shown in the left and right panels, respectively.
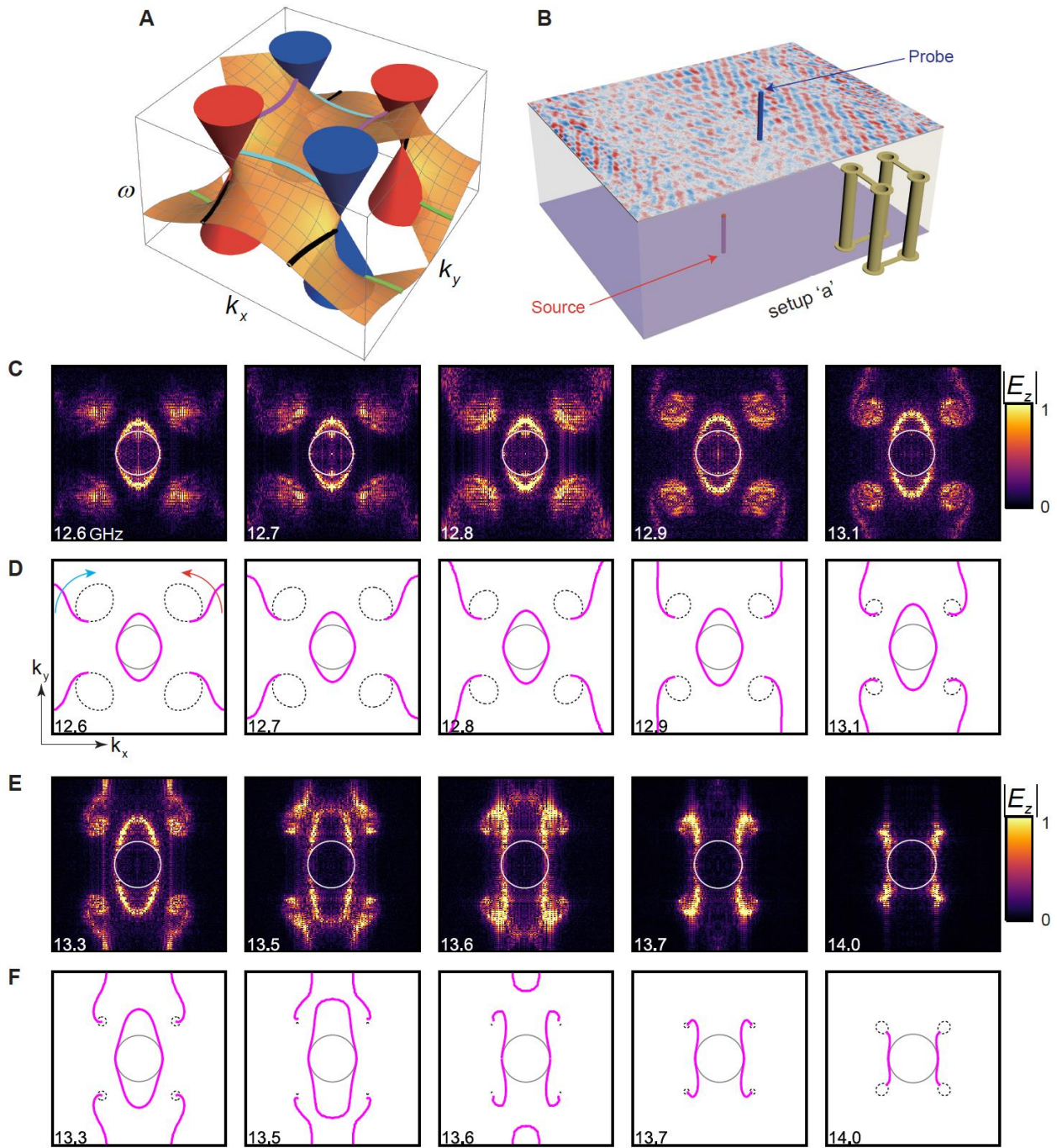
Fig. 3. Experimental observation of helicoidal structure of topological surface states. (A) Schematic illustration of helicoid surface states in an ideal Weyl system with four Weyl points within the surface Brillouin zone, plotted using the Jacobi elliptic function. The arcs of different colors represent the evolution of equi-frequency arcs connecting Weyl points of opposite Chern

numbers. (**B**) Transmitted near-field scanning system (setup 'a'), where the source (red) is positioned on the bottom surface center. (**C**) and (**E**) Equi-frequency contour ($|E_z|$) measured using setup 'a' from 12.6 GHz to 14.0 GHz. (**D**) and (**F**) Bulk (black dashed) and surface (magenta solid) states simulated by CST microwave studio, correspondingly. Anti-clockwise (red) and clockwise (cyan) arrows indicate the surface arc rotation directions with increasing frequency corresponding to positive and negative Weyl nodes, respectively. The central solid circle indicates the air equi-frequency contour. The plotted range for each panel is $[-\pi/a, \pi/a]^2$.

Supplementary Materials

Materials and Methods

Supplementary Text

Supplementary Figures S1-S6

References (*26-27*)